Carbon 173 (2021) 600–608

Contents lists available at ScienceDirect

Carbon

journal homepage: www.elsevier.com/locate/carbon

Research Article

The mechanical behavior and collapse of graphene-assembled hollow nanospheres under compression

Yifan Zhao [a, b, 1], Yushun Zhao [a, 1], Fan Wu [a, b, 1], Yue Zhao [a, b], Yaming Wang [f], Chao Sui [a], Xiaodong He [a, c], Chao Wang [d, e, *], Huifeng Tan [a, b, **], Chao Wang [a, ***]

[a] Center for Composite Materials and Structures, Harbin Institute of Technology, Harbin, 150080, PR China
[b] National Key Laboratory of Science and Technology for National Defence on Advanced Composites in Special Environments, Harbin Institute of Technology, Harbin, 150001, PR China
[c] Shenzhen STRONG Advanced Materials Research Institute Co., Ltd, PR China
[d] LNM, Institute of Mechanics, Chinese Academy of Sciences, Beijing, 100190, China
[e] School of Engineering Science, University of Chinese Academy of Sciences, Beijing, 100049, China
[f] Department of Materials Science, School of Materials Science and Engineering, Harbin Institute of Technology, Harbin, 150001, PR China

ARTICLE INFO

Article history:
Received 3 September 2020
Received in revised form
12 November 2020
Accepted 13 November 2020
Available online 16 November 2020

Keywords:
Graphene
Hollow nanosphere
In-situ test
Compressive mechanical properties

ABSTRACT

Recently, much interest has been attracted in the graphene-assembled hollow nanospheres (GAHNs) because of outstanding multi-functional properties. This paper systematically explores the compressive mechanical behaviors and gas bearing capability of GAHNs by a coarse-grained molecular dynamics (CGMD) simulation combining with in-situ compressive test. It was found that the GAHNs possess excellent compressive elasticity (experimentally recoverable strain can reach ~ 58%). Under large compressive strain (>90%), the GAHNs also display obvious plastic deformation owing to inter-layer slippage between graphene nanosheets. In addition, the morphology of force measurement tip (FMT) plays critical roles on the compressive failure modes of GAHNs. When FMT is sharp, it can pierce through the shell of GAHN, whereas the blunt one compels GAHN to collapse. The thermal expansion process of GAHNs was investigated by CGMD simulation. With the increase of ambient temperature, the internal pressure of GAHN increased until a crack appears. To further understand this expansion failure, an in-situ scratching experiment was designed and the tearing strength of shell of GAHN was estimated to be ~748 MPa. This work provides an in-depth understanding on intrinsic mechanical properties of GAHNs and broadens their potential applications.

1. Introduction

Since discovery in 2004, graphene has been seen as the most promising two-dimensional nanomaterial, due to its excellent mechanical, thermal and electrical properties, etc. [1,2] However, the small size and low-dimensional morphology of graphene limit its practical applications. A route to resolve this issue is that assembling nanoscale graphene into macroscopic bodies with unique multi-functional properties, such as graphene-based fibers, films and aerogels, etc. [3–9] Recently, much interest has been focused on a novel hierarchical structure, graphene-assembled hollow nanospheres (GAHNs), fabricated by solution or template methods. For example, Cao et al. [10] developed a one-step hydrothermal method, where the H_2SO_4 aqueous suspension was utilized to assemble graphene oxide nanosheets into hollow spheres. Su et al. [11] employed the silica spheres as templates to prepare the well-wrapped GAHNs with different number of shells. Compared to flat graphene, the spherical morphology of GAHNs possesses a larger accessible surface area for the adsorption of electrolyte and lithium ions, making them have great potential as supercapacitor [12–16], catalytic electrodes and oxygen reduction reaction catalyst [17–19], etc.

The mechanical properties of materials are the basics for their

* Corresponding author. LNM, Institute of Mechanics, Chinese Academy of Sciences, Beijing, 100190, China.
** Corresponding author. Center for Composite Materials and Structures, Harbin Institute of Technology, Harbin 150080, PR China.
*** Corresponding author.
E-mail addresses: wangchao@lnm.imech.ac.cn (C. Wang), tanhf@hit.edu.cn (H. Tan), chaowang@hit.edu.cn (C. Wang).
[1] These authors contributed equally.

https://doi.org/10.1016/j.carbon.2020.11.040
0008-6223/

practical applications. So far, the compressive mechanical behaviors of various solid and hollow nanospheres, correlated by their spherical nanostructures, have been studied by in-situ compression experiments combined with theoretical modelling. For examples, Chrobak et al. [20] found that solid Si nanosphere presented a dislocation-driven plasticity behavior under compression loading, which is different from phase transformation-driven plasticity of bulk Si. Shan group found that the spherical samples can effectively avoid surface dislocation nucleation of metal materials during compressive mechanical testing, by which the ideal strength of iron was obtained to be ~12 GPa [21]. Faerstein et al. [22] revealed remarkable high-stiffness property and outstanding recoverable elastic deformation capability of hollow boron nitride (BN) nanospheres. Inspired by biological shells and honeycomb-like cellular structures, Yang et al. [23] studied the compressive mechanical behaviors of one kind of amorphous carbon nanospheres. It was observed that this nanostructure can simultaneously exhibit high strength and large compression deformation. Meanwhile, an interesting delay-failure phenomenon of this nanostructure highly relating to the ratio of shell thickness and diameter was discovered [24]. Nevertheless, to our best knowledge, the compressive mechanical characteristics of GAHNs have not been in-depth explored yet.

It has been theoretically proved that some members of carbon family, such as fullerenes and carbon nanotubes, possess excellent pressure-resistant properties of gas [25–29]. Pupysheva et al. [30] studied the hydrogen storage capacity of ball-like fullerene nanocages using density functional theory. The general relationship between the internal pressure of the fullerene nanocages and C–C bond elongation was extracted. Manna et al. [31] calculated the gas (H_2 and CO_2) bearing capacity of nanocapsules consisting of single-walled carbon nanotubes with different chiralities by first principles calculations. Zhao et al. [25] designed an icosahedral fullerene structure with twelve pentagonal faces at the vertices of the regular icosahedron and twenty triangular faces. The molecular dynamics (MD) simulation results show that this extendible nanostructure with super-low density possesses excellent pressure resistance character. From the potential multi-functional application perspective of hollow carbon-based capsule structures, the thermal stability and gas bearing capacity of GAHNs have not been understood yet.

In this paper, we combine coarse-grained molecular dynamics (CGMD) simulation and in-situ scanning electron microscope (SEM) compressive tests to systematically study the compressive mechanical properties and thermal expansion properties of GAHNs for the first time. The super-compressive elasticity and plastic collapsing behavior of GAHNs were revealed. Moreover, we investigated the thermal expansion process and potential cracking failure mechanisms of gas-filled GAHNs. The tearing strength of GAHN shell was experimentally estimated to be ~748 MPa. This work provides an in-depth understanding on the intrinsic mechanical behaviors of graphene-based hollow nanospheres and broadens their applications.

2. Methods

2.1. Preparation of GAHNs

In this study, we prepared the GAHNs by a facile assembling method. At first, 10% HCl (v/v) was added into as-synthesized graphene oxide (GO) solution (2 mg mL^{-1}, 50 ml) to make the solution acidic, which introduce the GO nanosheets to self-curling. It is noted that the GO was synthesized by the improved Hummers' method [32]. Subsequently, the mixture was sonicated under ice bath for 0.5 h and then filtered by a filter membrane with a micropore size of 0.65 μm. The vacuum filtration provides the interlayer shearing force of graphene oxide sheet. After the above process, the free-standing GO paper is obtained which possesses surface microspheres with diameter of 30 mm. Then, the GO paper was suction-dried for 1 day firstly, and dried under vacuum at 80 °C for 2 h, and air-dried for 1–2 days under ambient conditions in the end. In this process, the graphene oxide curls to form carbon spheres. The X-ray photoelectron spectrum for as-prepared GAHN and the preparation process diagram are shown in Fig. S1, which character the structure of GAHN.

2.2. CGMD simulation

The large-scale atomic/molecular massively parallel simulator (LAMMPS) was employed to run all MD simulations in this work [33]. The related parameters of coarse-grained (CG) force field were chosen from the literature, which includes bonds, angles, dihedrals and non-bonded interactions [34]. Given that the Lennard-Jones (LJ) parameters ε_{LJ} and σ_{LJ} are 0.82 kcal/mol and 3.46 Å, respectively, and the cutoff distance between two adjacent graphene nanosheets (GNs) in GAHNs is 12 . We set the cutoff between substrate and GANH as 3.88 Å, as well as between the tip and GAHN. This value equals the distance corresponding to the lowest energy on the LJ potential, which effectively avoid unnecessary attraction of the substrate and the tip to GAHN. During the dynamics simulation, the system temperature was set to be 5 K to eliminate the unnecessary structural vibration caused by high temperature. The timestep was set to be 1 fs. The NVT (constant number of atoms N, constant volume V, and constant temperature T) ensemble was used during the whole simulation to guarantee the strcutural stablility of GAHNs. According to Martini's approach [35], the CG model was constructed by hexagonal lattice of beads, where each bead represented four atoms in fully atomic model of GNs, as shown in Fig. 1a. All GNs in the initial configuration are randomly distributed in the simulation box, and a spherical boundary with a radius of 5000 Å expressed by R_i shrinks inward in a constant speed to push the sheets into a ball, as shown in Fig. 1b. There is a fixed spherical area where no sheet exists in the middle of the simulation box to guarantee the hollow structure. As the boundary continues to shrink, the graphene sheets overlap each other until it is assembled into a hollow sphere. The resulting GAHN model was built by 84 CG graphene nanosheets with a same size of 200 Å × 200 Å, which totally contains 330,624 carbon beads.

2.3. In-situ SEM compression testing

We employed a sensitive force measurement system (FMS) to study the cyclic compression behaviors of GAHNs and achieve tearing strength of GAHNs (Kleindiek Nanotechnik, Germany). The FMS is composed of a nano-manipulator equipped with an force measurement tip (FMT) and force output system. There is a piezoelectric force sensor between nano-manipulator and FMT. The force measurement resolusion of FMT and the moving resolution of the nano-manipulator are ~1 nN and ~0.25 nm, respectively. Two kinds of FMTs, sharp and blunt, were used in experiments to investigate their effect on compressive mechanical behaviors. Before testing, the nano-manipulator with FMT and GAHN samples were fixed into the chamber of SEM. Subsequently, the FMT was calibrated by a calibration spring, during which it was moved down until the calibration spring has been bent to the 1.0 μm mark, as shown in Fig. S2. After calibration, the force value for the next experiment will be calculated by software based on the voltage transmitted by the piezoelectric sensor and the parameters of the calibration beam. The testing force-time curve can be directly output, and the force-displacement curve can be extracted by the

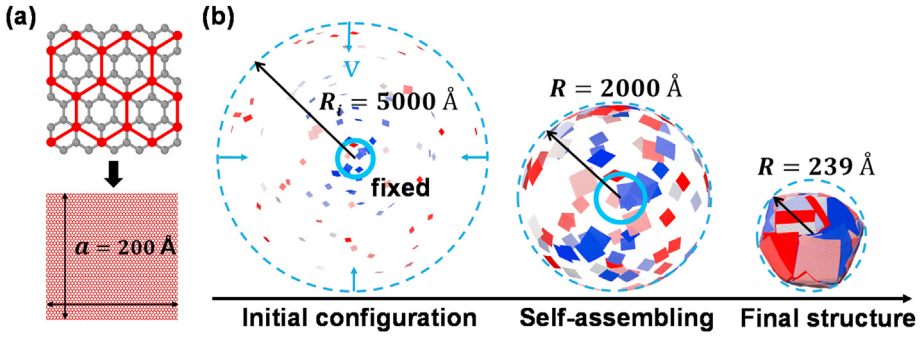

Fig. 1. (a) A schematic for demonstrating the CG process for graphene GNs. (b)The modeling process of GAHN. (A colour version of this figure can be viewed online.)

force-time curve combining with in-situ testing video.

3. Results and discussion

In this study, the parameters of CG force field were chosen from a classic literature, where the mechanical responses of graphene can be accurately estimated [34]. In details, a Morse function was used to describe the bond potential term in the CG models:

$$V_b(d) = D_0\left[1 - e^{-\alpha(d-d_0)}\right]^2 \quad (1)$$

where D_0 and α are force constants, and d_0 is the equilibrium bond length. A harmonic function was used to describe the angle potential term:

$$V_a(\theta) = k_\theta(\theta - \theta_0)^2 \quad (2)$$

where k_θ is the spring constant and θ_0 is the equilibrium angle. And another harmonic function was used to describe the dihedral potential term:

$$V_d(\varnothing) = k_\varnothing[1 - cos(2\varnothing)] \quad (3)$$

where k_Φ is the spring constant. The non-bonded van der Waals (vdW) interaction force between GNs was described by a LJ potential [36]:

$$V_{nb}(r) = 4\varepsilon_{LJ}\left[\left(\frac{\sigma_{LJ}}{r}\right)^{12} - \left(\frac{\sigma_{LJ}}{r}\right)^{6}\right] \quad (4)$$

where ε_{LJ} is the depth of the potential well, which can reflect the strength of the attraction between two beads. σ_{LJ} is the LJ parameter associated with the equilibrium distance between two non-bonded beads. And r is the bead-to-bead distance in a cutoff range.

Based on the force field relationship above, we obtained GAHN model by the method of MD simulation. Fig. 2a and b show the final configuration of a GAHN, besides, the radius R and average thickness t are ~239 Å and ~20 Å, respectively. In addition, we also prepared a kind of GAHN by a simple solusion method (see detailed preparation method in the Methods), which has the same structure depicted in molecular model (Fig. 2d and e). To peform the following theoretical prediction, the prepared GAHNs were used in the in-situ compression and scratching testing. Fig. 2c and f show the same laminated nanostructure of the molecular models and experimental samples, where GNs are overlapped each other.

To study the compressive mechanical properties of GAHNs, the compressive force F versus displacement δ is defined as shown in Fig. 3a. To be consistent with the loading mode in in-situ experiment, we constructed the cone-like diamond tip to compress GAHN. The bluntness degree of tip is described by the parameter r_{tip} and h, which are the radius and the height of tip, respectively. During the simulation, the parameter h is constant, so a sharper tip has a smaller r_{tip}, and vice versa. The GAHN was placed on a rigid plate composed of three layers of flat GNs to achieve the compression loading. Fig. 3b shows the three cyclic loading curves with different compression strain ε, where taking r_{tip} = 6 Å and compression velocity v_c = 5 m/s, respectively. It is noted that ε is calculted by $\varepsilon = \delta/2R$, where R is the outer radius of GAHN, δ is the displacement of the contant point between the tip and GAHN. It can be seen that, during the first two cycles of loading, the unloading curves can retract along loading path, with a full storage-release process of internal stress, indicating a good compressive elasticity. The fluctuations in the curves exactly reflect the deformation response of this multilayer self-assembled hollow structure under compressive load. When ε increases to 30%, as shown in Fig. 3b and c, there has been a slight degree of plastic deformation in the structural deformation process. We selected several adjacent GNs colored by red, yellow and blue near the tip to further realize the structural evolution of GAHN during the third compression-recovery cycle (Fig. 3d). As the tip moves down and continually compresses the ball, the red and yellow GNs are gradually sunken, while the blue one keeps its original position. Whereas, when the tip is raised, the blue GN rotates and slips to one side sligthly to reach the deformation coordination of the structure. During this process, the interfacial vdW interaction between GNs dominates the strcutural stability. The most of external compressive work can be effectively transferred to elastic deformation energy of GNs, but a small part is consumed in the slipping between layers. Hence the elastic deformation mechanism supplemented by plastic deformation is revealed in the third compression-recovery process. Considering that the plastic deformation of overall structure is tiny, as shown in Fig. 3c, this structure can still be regarded as superelasticity nanosphere. Moreover, an interesting bouncing phenomenon was observed because of a fast release of elastic deformation energy after completely unloading (Video S1).

We further investigated the cyclic compressive mechanical behavior of GAHN under a compressive strain of up to 90% (Fig. 4, Video S2). Five feature points were selected from the F-δ curve to depict the whole structural evolution process (Fig. 4a), combining with corresponding compressive snapshots (Fig. 4b and c). It can be seen that before point a, there is a linear relationship between F and δ, indicating a pure elastic deformation. Between point a and b, the structure has undergone both elastic and plastic deformation. As the displacement increases continuely, it goes into a plastic yielding stage (between point b and c), where F does not increase but keeps a fluctuation state. After point c, the structure is gradually unloaded and cannot fully recover to its original configuration (Fig. 4b). The evolution of the four GNs selected in the red square in Fig. 4b is

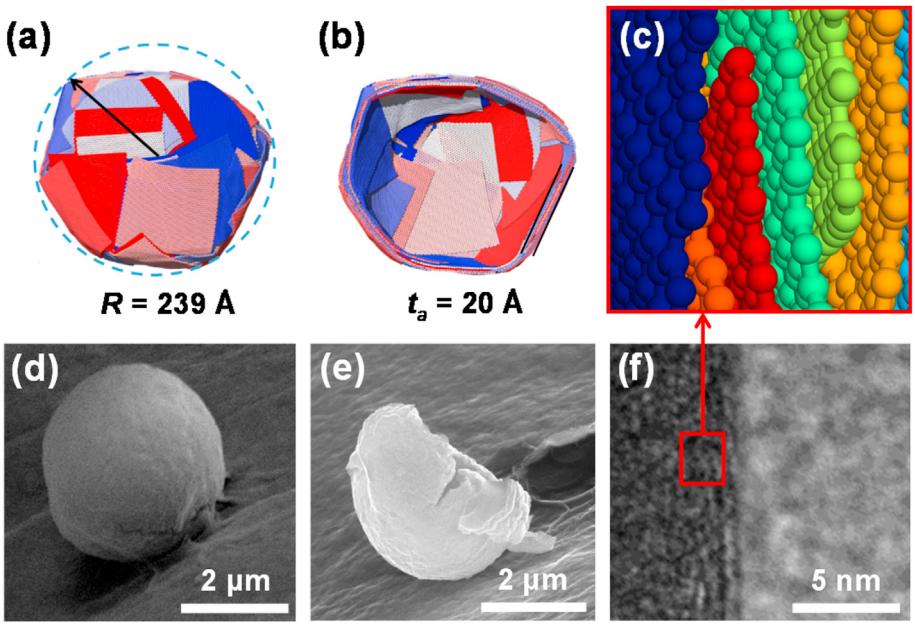

Fig. 2. (a)–(b) The final configuration of the GAHN. (d)–(e) The SEM images of GAHNs. (f) A transmission electron microscope (TEM) image for the cross-section of shell of GAHN. The lamination structure of GAHN in the red square is shown by (c) the enlarged molecular dynamics diagram. (A colour version of this figure can be viewed online.)

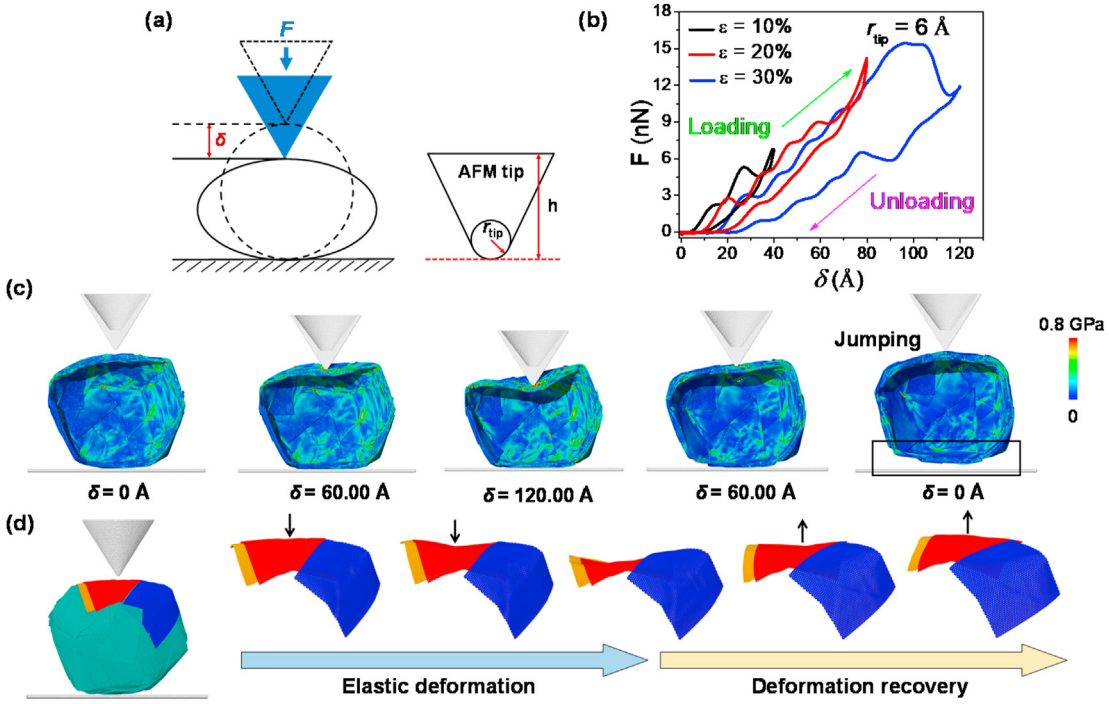

Fig. 3. (a) A schematic of tip, compressive loading *F* and displacement *δ*. (b) The cyclic compression force *F* versus displacement *δ* curves with different compressive strains. (c) The snapshots of GAHN under the third cyclic compressive loading (compression strain is 30%). (d) Corresponding evolution process of local structure of GAHN under the third cyclic loading. (A colour version of this figure can be viewed online.)

enlarged and shown in Fig. 4c. At the beginning, the blue GN is bent first, and the structure is in an elastic deformation stage. Gradually, the slipping and bending become obvious. After point *b* (δ = 169.48 Å), the top blue GN is pressed into the ball with the movement of tip, and the bending deformation is extended to the adjacent yellow and indigo GNs. When δ reaches 313.98 Å, an interlocking between the four GNs can be clearly observed from another perspective, as shown in the red dashed square. The structural buckling of GAHN shell with large bending deformation and inter-layer slippage of GNs is irreversible, which results in a plastic deformation. Therefore, the recovery of the four GNs is unobvious during the unloading process. This deformation mechanism is different from that of hollow BN nanoparticles controlled by interlayered bonds and structural phase transition [22].

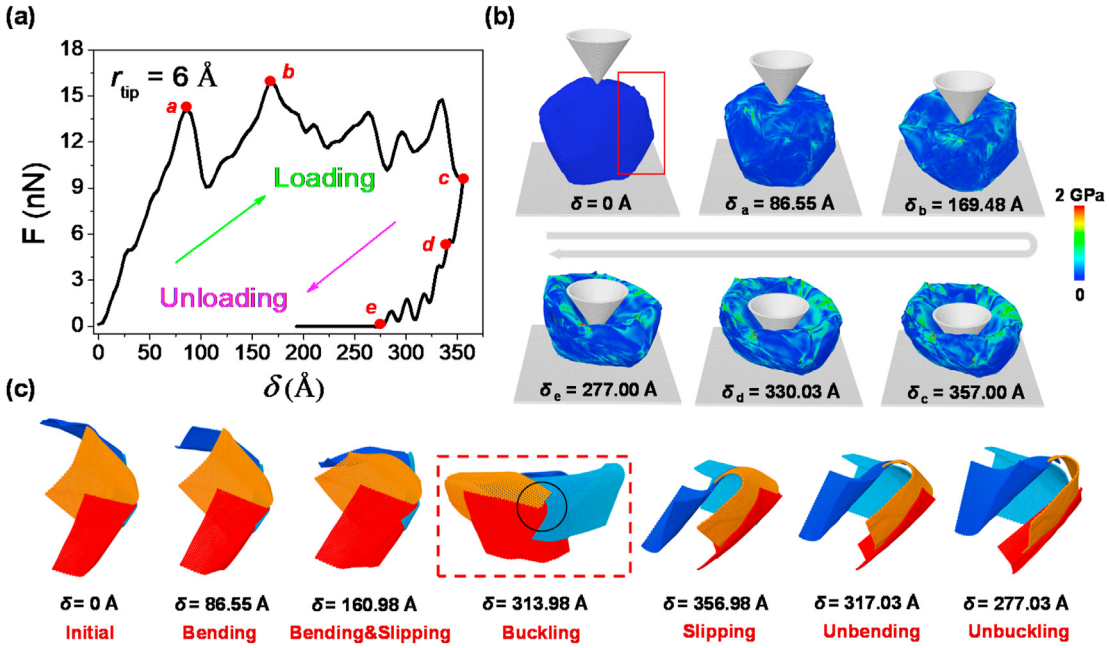

Fig. 4. (a) The compression force *F* versus displacement *δ* curve when compressive strain is up to 90%. (b) The snapshots of GAHN under cyclic loading. (c) Corresponding evolution process of local structure of GAHN under cyclic loading. (A colour version of this figure can be viewed online.)

Besides the insights of MD simulations, we performed the in-situ SEM compressive test to study the cyclic compressive behaviors of GAHNs as well, by which the structural changes of hollow nanosphere under loading can be well observed [22,37]. As shown in Fig. 5a, we utilized the FMT to compress a GAHN, and the *F*-*δ* curve for whole cyclic loading is shown in Fig. 5b. It is noted that the initial position of cantilever of FMT needs to be parallel to the horizontal plane. Considering that the rotation angle of cantilever of FMT is much smaller than its length, therefore, the loading direction is regarded as passing through the centre of sphere and the tangency point of sphere and horizontal plane. As the diameter of GAHN is ~2.8 μm, the maximum compression displacement was set to be ~2.2 μm (corresponding compression strain is 78%). The detailed experimental setup can be found in the Methods. It can be observed that the local sunken deformation of GAHN was gradually formed with an increase of *δ* (Fig. 5c, Video S3). During unloading stage, the structure with a partial sunken was recovered. When FMT was completely away from GAHN, an ellipsoid morphology with residual deformation of ~20% was left, by which we can deduce that the elastic recovery strain is approximately 58%. Although it is difficult to directly reveal the origin of plastic deformation by in-situ SEM observation, it is reasonable to explain deformation mechanism by the inter-layer slipage failure between GNs from MD simulation.

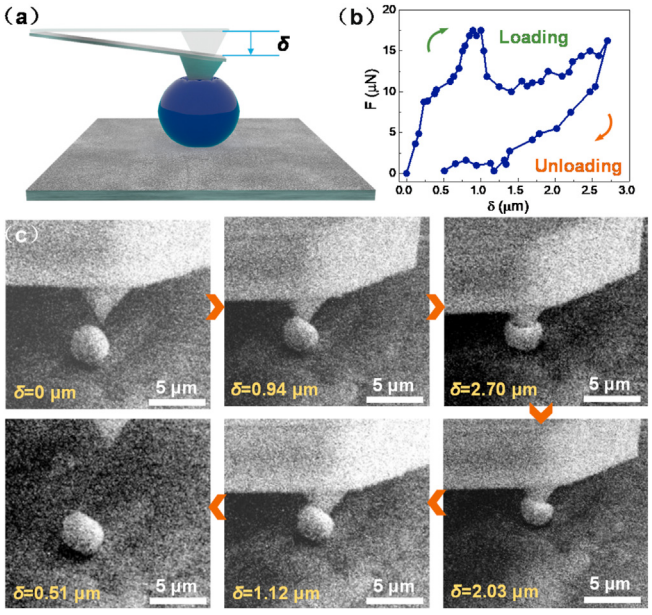

Fig. 5. (a) A schematic of in-situ compression test for a GAHN. (b) The *F*-*δ* curve of a GAHN with diameter of 2.8 μm under cyclic loading (compressive strain is 78%). (c) Corresponding snapshots under the whole cyclic loading. (A colour version of this figure can be viewed online.)

The effect of the tip morphology on compressive mechanical behaviors of GAHNs was investigated as well, where the radius r_{tip} = 1.5 Å and r_{tip} = 30 Å represent for a sharp and blunt tips, respectively (Fig. 6a). From the responses of *F*-*δ*, there are similar deformation trends before structure failure, including pure linearly elastic deformation (before *a* and *a′*) and elastic-plastic deformation (*a*-*b* and *a′*-*b′*). However, it can be observed that there are two distinct different failure modes. When the tip is sharp, it can pierce through the shell of GAHN from the weak joints or gaps between GNs (Fig. 6c and d), leading to a decline of *F*. This behavior was also experimentally validated that a sharp FMT could directly pierce out from the GNs (Fig. 6e). In contrast, the blunt tip causes a collapsing failure (Fig. 6f), which can be explained by the contact area between blunt tip and GAHN is relatively large. With the increase of compressive strain, the shell of GAHN is gradually flattened until the upper and lower parts are attracted together by vdW interaction (Fig. 6g and h). When it comes to a flat tip, namely, $r_{tip} = \infty$, as shown in Fig. S3, the compression strength σ_c of GAHN can be theoretically estimated to be 1.14 GPa by $\sigma_c = F_{cmax}/S_c$. The F_{cmax} is the maximum compression force before structure collapsing (point b′), and S_c is the true contact area between plate and GAHN, which is estimated by determining the number of carbon beads on GAHN

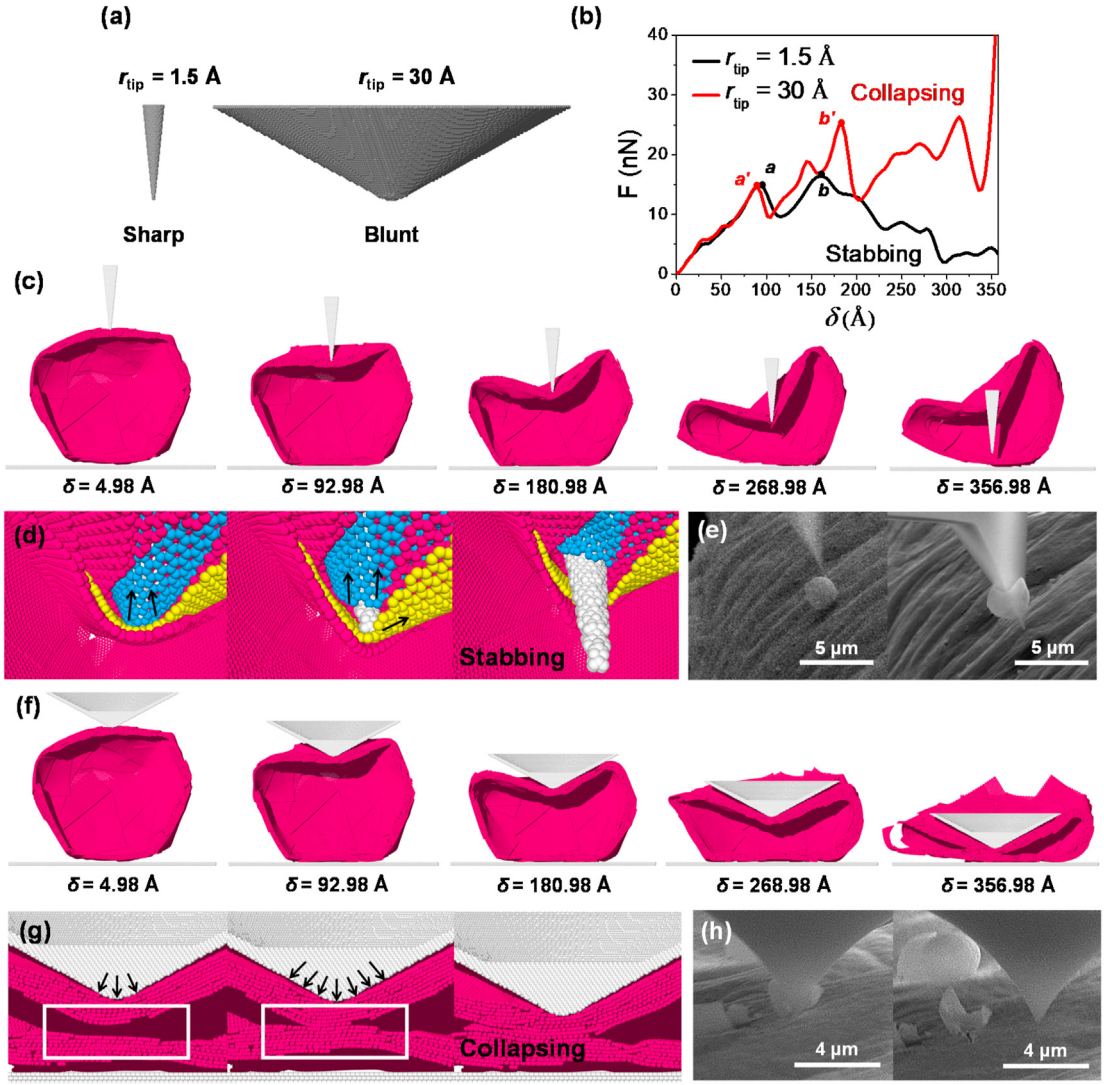

Fig. 6. (a) The sharp and blunt tips, the radius are 1.5 Å and 30 Å, respectively. (b) The curves of the compressive force *F* versus displacement *δ* using different tips. (c) The process of piercing through the shell of GAHN using a sharp tip from CGMD simulation. (d) Local configuration after piercing the shell of GAHN, where the tip is passed through from the gaps between GNs. (e) The SEM images before and after piercing through a GAHN using a sharp triangular FMT. (f) The process of collapsing a GAHN using a blunt tip from CGMD simulation. (g) Local collapsed configuration of GAHN. (h) The SEM images for a collapsed GAHN using a blunt FMT. (A colour version of this figure can be viewed online.)

experiencing a non-zero vdW interaction with the plate [20].

There are many studies investigated the ultra-light materials, whose density is infinitely close to air but not really lower than air [38,39]. Based on this background, we carried out research on the real floating property of the prepared hollow structure. Following the above study on the intrinsic mechanical properties, we first explored the thermal stability and gas bearing capability of GAHNs. One of the most stable gas, helium, was employed in the simulation. In order to simplify modelling, the same CG strategy was utilized for helium, where each CG helium bead represented four actual helium atoms, and total 5000 CG helium beads were filled into the GAHN (Fig. 7a). Since there is no accurate LJ parameters to describe the interaction betwee CG helium beads and CG carbon beads, and the focus of this work is the thermal stability and corresponding failure mechanisms of GAHN, the same LJ parameters was employed to approximately depict the interaction of helium beads and carbon beads.

Fig. 7b shows the relationship curve of internal pressure *P* and temperature *T*. The *P* is calculated by $P = F_i/V_d$, where F_i is the force caused by the interaction between inwall of GAHN and helium beads, and V_d is the effective diffused volume of helium beads. In the initial state, helium beads forms a cluster in the center of GAHN (Fig. 7a). With gradual increase of *T*, the cluster of helium begins to diffuse outwards, resulting in a slight increase of *P* (below 30 K). When the temprerature is between 30 K and 137 K, *P* further increases. Meanwhile, the surface of GAHN keeps moving under the action of the expanded helium and the continuely increased temprature, a crack gradually appeared, as shown in Fig. 7c. During this stage, due to the internal space is still not fully filled with helium beads, the helium beads do not leak immediatliy but continues to expand with the increase of temperature. When *T* exceeds to 137 K, the gas particles leaked from the crack and the internal pressure *P* begins to decline. At the same time, the crack becomes narrow and stable owing to the decrease of gas volume. The thermal expansion process can be seen in Video S4.

The thermal stability and gas bearing capacity of GAHN obtained in MD simulation during the heating process are related to the actual tearing strength of shell of the structure. In order to realize the intrinsic mechanical strength of shell, a scratching experiment is designed for the GAHNs using FMT. The loading position of FMT is

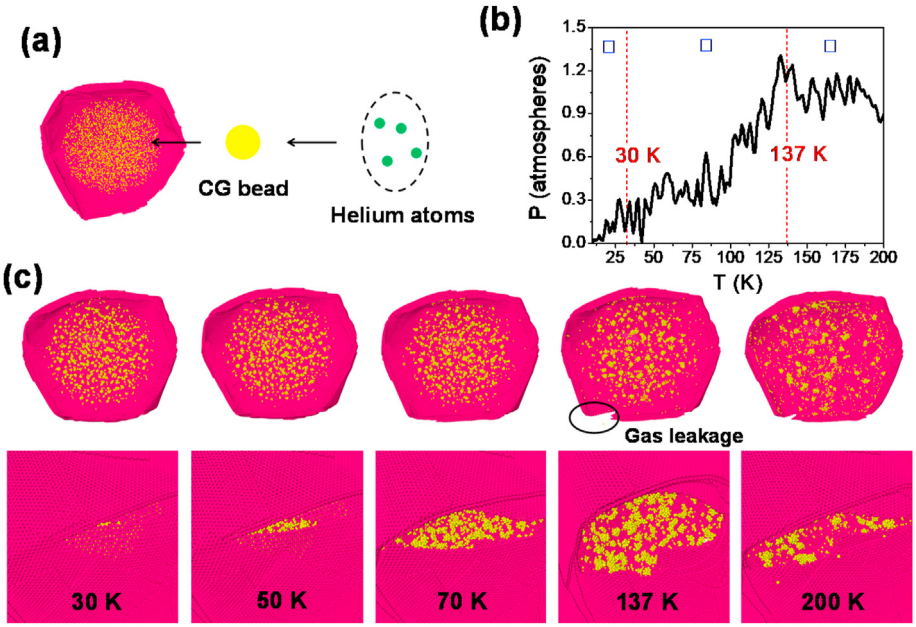

Fig. 7. (a) An initial configuration of GAHN filled with helium, where four helium atoms are equivalent to one CG bead. (b) The relationship between internal pressure *P* and temperature *T*, which can be divided into three stages. (c) The sectional morphologies of a GAHN filled with helium under different *T*, and evolution process of local crack propagation of GAHN shell. (A colour version of this figure can be viewed online.)

adjusted intentionally from centre to the edge of GAHN by controling the nanomanipulator, as shown in Fig. 8a. Fig. 8b shows the curve of deviated compression loading versus displacement of GAHN with a diameter of 2.74 μm, where the deviation distance *D* is approximately 1.43 μm. The corresponding snapshots are presented in Fig. 8c. With the increase of compressive displacement, a local collapsed deformation near FMT can be clearly observed. When the loading almost reaches to the maximum values (35 μN), a sudden slippage of FMT towards down was observed. Meanwhile, a scratching crack is formed and some teared-off GNs are retained on FMT after unloading. The scratching process can be seen in Video S5. The tearing strength is defined in this paper with $\sigma_t = F_{cmax}/S = F_{cmax}/(2Lt)$, where $S = 2Lt$ is cross-section area of the long and narrow crack which is approximately regarded as two rectangular surfaces, $L = 1.17$ μm and $t = 20$ nm are the length and thickness of crack, respectively (Fig. 8d). According to the above relationship, the σ_t was approximately estimated to be 747.86 MPa. Although this value cannot be directly compared with the tensile strength of

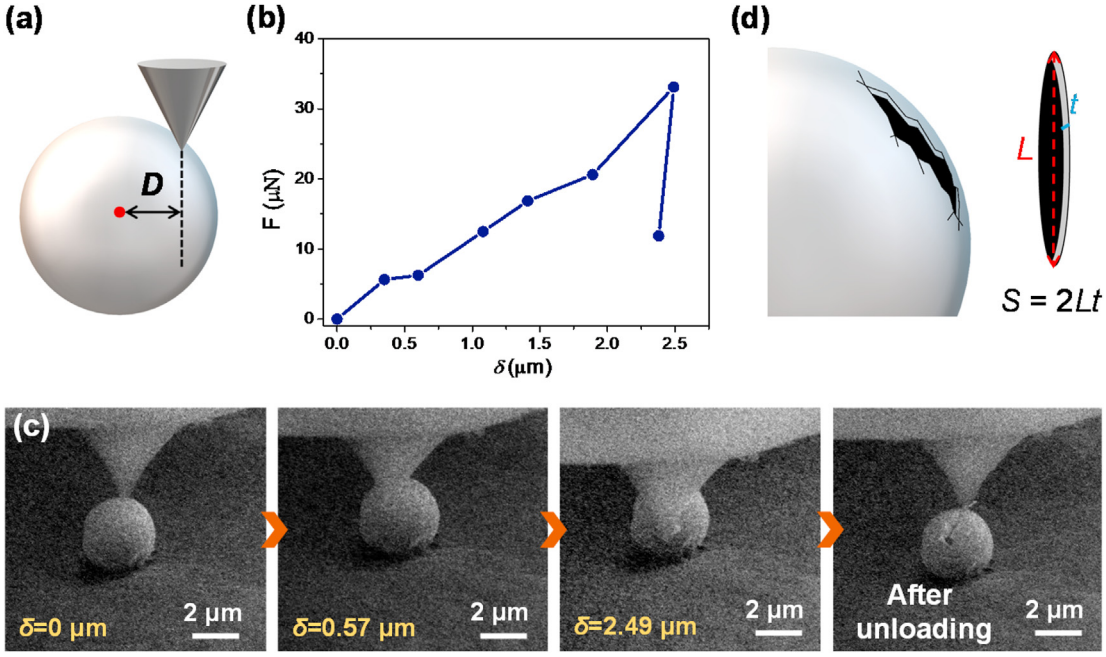

Fig. 8. (a) A schematic for deviated compressive loading. (b)–(c) Deviated compression force versus displacement curve of a GAHN with diameter of 2.74 μm and corresponding snapshots, where an obvious scratched crack can be observed. (d) A schematic of approximate calculation of crack area. (A colour version of this figure can be viewed online.)

graphene-based papers/films, they are in the same order of magnitude based on the vdW interaction [40–43].

4. Conclusion

This work investigates the compressive mechanical responses and thermal expansion process of GAHNs by CGMD simulation combining with in-situ SEM experiments. Both theoretical and experimental results show that GAHNs have an excellent elasticity within relatively small compressive strain (maximum value is ~58%), and the structure behaves an interesting bouncing phenomenon due to a fast release of elastic deformation energy. When the compressive strain is up to 90%, the structure displays irreversible plastic deformation, owing to the large buckling of GNs and inter-layer slippage between GNs. Additionally, we found two typical structure failure modes of GAHNs, piercing and collapsing, depending on the morphology parameter r_{tip}. At last, the CGMD simulation reveals that the gas expansion can crack the GAHNs. And the tearing strength of GAHNs, which reflect the intrinsic mechanical performance, was estimated to be ~748 MPa by an in-situ scratching experiment. This work lays the foundation for the multi-functional applications of GAHNs.

CRediT authorship contribution statement

Yifan Zhao: Methodology, Software, Investigation, Writing - original draft. **Yushun Zhao:** Methodology, Formal analysis, Investigation. **Fan Wu:** Methodology. **Yue Zhao:** Methodology. **Yaming Wang:** Methodology. **Chao Sui:** Project administration, Funding acquisition. **Xiaodong He:** Conceptualization, Supervision, Funding acquisition. **Chao Wang:** Conceptualization, Supervision, Resources. **Huifeng Tan:** Conceptualization, Supervision, Funding acquisition. **Chao Wang:** Conceptualization, Supervision, Funding acquisition, Resources, Writing - review & editing.

Declaration of competing interest

The authors declare that they have no known competing financial interests or personal relationships that could have appeared to influence the work reported in this paper.

Acknowledgments

This work was financially supported by the National Natural Science Foundation of China (Grant No. 11872164, 51702064), National Key Research and Development Program of China (Grant No. 2018YFA0702802). Shenzhen Science and Technology Program (Grant No. KQTD2016112814303055).

Appendix A. Supplementary data

Supplementary data to this article can be found online at https://doi.org/10.1016/j.carbon.2020.11.040.

References

[1] C. Lee, X.D. Wei, J.W. Kysar, J. Hone, Measurement of the elastic properties and intrinsic strength of monolayer graphene, Science 321 (2008) 385–388.
[2] A.A. Balandin, S. Ghosh, W.Z. Bao, I. Calizo, D. Teweldebrhan, F. Miao, et al., Superior thermal conductivity of single-layer graphene, Nano Lett. 8 (2008) 902–907.
[3] A.V. Melechko, V.I. Merkulov, T.E. McKnight, M.A. Guillorn, K.L. Klein, D.H. Lowndes, et al., Vertically aligned carbon nanofibers and related structures: controlled synthesis and directed assembly, J. Appl. Phys. 97 (2005) 3–165.
[4] M. Inagaki, Y. Yang, F.Y. Kang, Carbon nanofibers prepared *via* electrospinning, Adv. Mater. 24 (2012) 2547–2566.
[5] A. Ramos, I. Camean, A. B. Garcia Graphitization, Thermal treatment of carbon nanofibers, Carbon 59 (2013) 2–32.
[6] S. Nardecchia, D. Carriazo, M.L. Ferrer, M. Gutierrez, F. Monte, Three dimensional macroporous architectures and aerogels built of carbon nanotubes and/or graphene: synthesis and applications, Chem. Soc. Rev. 42 (2012) 794–830.
[7] J.H. Zou, J.H. Liu, A.S. Karakoti, A. Kumar, D. Joung, Q.A. Li, et al., Ultralight multiwalled carbon nanotube Aerogel, ACS Nano 4 (2010) 7293–7302.
[8] X.T. Zhang, Z.Y. Sui, B. Xu, S.F. Yue, Y.J. Luo, W.C. Zhan, et al., Mechanically strong and highly conductive graphene aerogel and its use as electrodes for electrochemical power sources, J. Mater. Chem. 21 (2011) 6494–6497.
[9] M.A. Worsley, T.Y. Olson, J.R.I. Lee, T.M. Willey, M.H. Nielsen, S.K. Roberts, et al., High surface area, sp^2-cross-linked three-dimensional graphene monoliths, J. Phys. Chem. Lett. 2 (2011) 921–925.
[10] J.Y. Cao, Y.M. Wang, P. Xiao, Y.C. Chen, Y. Zhou, J.H. Ouyang, et al., Hollow graphene spheres self-assembled from graphene oxide sheets by a one-step hydrothermal process, Carbon 56 (2013) 389–391.
[11] F.B. Su, X.S. Zhao, Y. Wang, L.K. Wang, J.Y. Lee, Hollow carbon spheres with a controllable shell structure, J. Mater. Chem. 16 (2006) 4413–4419.
[12] J.S. Lee, S.I. Kim, J.C. Yoon, J.H. Jang, Chemical vapor deposition of mesoporous graphene nano-balls for supercapacitor, ACS Nano 7 (2013) 6047–6055.
[13] Z.C. Yang, C.H. Tang, Y. Zhang, H. Gong, X. Li, J. Wang, Cobalt monoxide-doped porous graphitic carbon microspheres for supercapacitor application, Sci. Rep. 3 (2013).
[14] C.W. Huang, C.H. Hsu, P.L. Kuo, C.T. Hsieh, H.S. Teng, Mesoporous carbon spheres grafted with carbon nanofibers for high-rate electric double layer capacitors, Carbon 49 (2011) 895–903.
[15] X.M. Ma, M.X. Liu, L.H. Gan, Y.H. Zhao, L.W. Chen, Synthesis of micro- and mesoporous carbon spheres for supercapacitor electrode, J. Solid State Electrochem. 17 (2013) 2293–2301.
[16] Q.G. Shao, J. Tang, Y.X. Lin, F.F. Zhang, J.S. Yuan, H. Zhang, et al., Synthesis and characterization of graphene hollow spheres for application in supercapacitors, J. Mater. Chem. 1 (2013) 15423–15428.
[17] S.M. Yoon, W.M. Choi, H. Baik, H.J. Shin, I. Song, M.S. Kwon, et al., Synthesis of multilayer graphene balls by carbon segregation from nickel nanoparticles, ACS Nano 6 (2012) 6803–6811.
[18] P. Guo, H.H. Song, X.H. Chen, Hollow graphene oxide spheres self-assembled by W/O emulsion, J. Mater. Chem. 20 (2010) 4867–4874.
[19] L.F. Wu, H.B. Feng, M.J. Liu, K.X. Zhang, J.H. Li, Graphene-based hollow spheres as efficient electrocatalysts for oxygen reduction, Nanoscale 5 (2013) 10839–10843.
[20] D. Chrobak, N. Tymiak, A. Beaber, O. Ugurlu, W.W. Gerberich, R. Nowak, Deconfinement leads to changes in the nanoscale plasticity of silicon, Nat. Nanotechnol. 6 (2011) 480–484.
[21] W.Z. Han, L. Huang, S. Ogata, H. Kimizuka, Z.C. Yang, C. Weinberger, et al., From "smaller is stronger" to "Size-Independent strength plateau": towards measuring the ideal strength of iron, Adv. Mater. 27 (2015) 3385–3390.
[22] K.L. Firestein, D.G. Kvashnin, A.M. Kovalskii, Z.I. Popov, P.B. Sorokin, D.V. Golberg, et al., Compressive properties of hollow BN nanoparticles: theoretical modeling and testing in a high-resolution transmission electron microscope, Nanoscale 10 (2018) 8099–8105.
[23] W.Z. Yang, S.M. Mao, J. Yang, T. Shang, H.G. Song, J. Mabon, et al., Large-deformation and high-strength amorphous porous carbon nanospheres, Sci. Rep. 6 (2016).
[24] W.Z. Yang, J. Yang, Y.Z. Dong, S.M. Mao, Z.Z. Gao, Z.F. Yue, et al., Probing buckling and post-buckling deformation of hollow amorphous carbon nanospheres: *In situ* experiment and theoretical analysis, Carbon 137 (2018) 411–418.
[25] Y.F. Zhao, Y. Lian, H.F. Tan, Study on the icosahedral fullerene structure with ultra-light and pressure resistance characters, Phys. Chem. Chem. Phys. 21 (2019) 11748–11754.
[26] P.H. Ying, Y.F. Zhao, H.F. Tan, Study on collapse controlling of single-wall carbon nanotubes by helium storage, Comput. Mater. Sci. 164 (2019) 133–138.
[27] V. Georgakilas, J.A. Perman, J. Tucek, R. Zboril, Broad family of carbon nanoallotropes: classification, chemistry, and applications of fullerenes, carbon dots, nanotubes, graphene, nanodiamonds, and combined superstructures, Chem. Rev. 115 (2015) 4744–4822.
[28] R.E. Tuzun, D.W. Noid, B.G. Sumpter, R.C. Merkle, Dynamics of He/C60 flow inside carbon nanotubes, Nanotechnology 8 (1997) 112–118.
[29] W.W. Cui, T.F.T. Cerqueira, S. Botti, M.A.L. Marques, A. San-Miguel, Nanostructured water and carbon dioxide inside collapsing carbon nanotubes at high pressure, Phys. Chem. Chem. Phys. 18 (2016) 19926–19932.
[30] O.V. Pupysheva, A.A. Farajian, B.I. Yakobson, Fullerene nanocage capacity for hydrogen storage, Nano Lett. 8 (2008) 767–774.
[31] A.K. Manna, S.K. Pati, Stability and electronic structure of carbon capsules with superior gas storage properties: a theoretical study, Chem. Phys. 426 (2013) 23–30.
[32] W.S. Hummers Jr., R.E. Offeman, Preparation of graphitic oxide, J. Am. Chem. Soc. 80 (1958), 1339–1339.
[33] S. Plimpton, Fast parallel algorithms for short-range molecular dynamics, J. Comput. Phys. 117 (1995) 1–19.
[34] L. Ruiz, W.J. Xia, Z.X. Meng, S. Keten, A coarse-grained model for the mechanical behavior of multi-layer graphene, Carbon 82 (2015) 103–115.
[35] S.J. Marrink, H.J. Risselada, S. Yefimov, D.P. Tieleman, A.H. de Vries, The MARTINI force field: coarse grained model for biomolecular simulations,

J. Phys. Chem. B 111 (2007) 7812–7824.
[36] J.E. Jones, On the determination of molecular fields. II. From the equation of state of a gas, Proc. R. Soc. 106 (1924) 463–477.
[37] J. Deneen, W.M. Mook, A. Minor, W.W. Gerberich, C.B. Carter, In situ deformation of silicon nanospheres, J. Mater. Sci. 41 (2006) 4477–4483.
[38] H.Y. Sun, Z. Xu, C. Gao Multifunctional, Ultra-flyweight, synergistically assembled carbon aerogels, Adv. Mater. 25 (2554) (2013) 2554–2560.
[39] Y.J. Meng, T.M. Young, P.Z. Liu, C.I. Contescu, B. Huang, S.Q. Wang, Ultralight carbon aerogel from nanocellulose as a highly selective oil absorption material, Cellulose 22 (435) (2015) 435–447.
[40] D.A. Dikin, S. Stankovich, E.J. Zimney, R.D. Piner, G.H.B. Dommett, G. Evmenenko, et al., Preparation and characterization of graphene oxide paper, Nature 448 (2007) 457–460.
[41] H. Chen, M.B. Mueller, K.J. Gilmore, G.G. Wallace, D. Li, Mechanically strong, electrically conductive, and biocompatible graphene paper, Adv. Mater. 20 (2008) 3557–3561.
[42] C.M. Chen, Q.H. Yang, Y.G. Yang, W. Lv, Y.F. Wen, P.X. Hou, et al., Self-assembled free-standing graphite oxide membrane, Adv. Mater. 21 (2009) 3007–3011.
[43] Y.W. Zhu, S. Murali, W.W. Cai, X.S. Li, J.W. Suk, J.R. Potts, et al., Graphene and graphene oxide: synthesis, properties, and applications. Advanced materials, Adv. Mater. 22 (2010) 3906–3924.